ChemComm

COMMUNICATION

View Article Online
View Journal | View Issue

Cite this: *Chem. Commun.*, 2022, **58**, 3673

Received 29th November 2021,
Accepted 16th February 2022

DOI: 10.1039/d1cc06701j

rsc.li/chemcomm

DNA origami nanocalipers for pH sensing at the nanoscale†

Xinyue Zhang,‡[ab] Li Pan,‡[ac] Ruiyan Guo,[a] Yueyue Zhang,[a] Fan Li,[a] Min Li,[a] Jiang Li,[d] Jiye Shi,[d] Fengli Qu,[b] Xiaolei Zuo[ac] and Xiuhai Mao*[a]

A DNA origami nanocaliper is employed as a shape-resolved nanomechanical device, with pH-responsive triplex DNA integrated into the two arms. The shape transition of the nanocaliper results in a subtle difference depending on the local pH that is visible *via* TEM imaging, demonstrating the potential of these nanocalipers to act as a universal platform for pH sensing at the nanoscale.

pH, which represents the activity of hydrogen ions (H^+) in solution, is one of the few chemical parameters that has widespread effects on the thermodynamics and kinetics of chemical reactions in the aqueous phase and at interfaces.[1–3] The charges of molecules or clusters, in particular, can alter the diffusion layer pH compared with the surrounding environment, resulting in unique chemical and physical properties.[4–6] Due to the confined surface electric charges of natural enzymes and nanoparticles, they exhibit pH-dependence during biological processes such as denaturation, catalysis, and delivery.[7,8] Thus, the ability to sense pH at the nanoscale is critical for understanding the role of pH in a variety of chemical and biological reactions, including electrocatalysis, biochemical engineering, cell biology, and biomedicine.[9,10]

Among the various pH sensing systems,[11–14] DNA-based pH sensors have attracted much attention due to their programmability in terms of their operational characteristics.[15–17] In general, these pH sensors are composed of two modules: a spectroscopic reporter and pH-responsive nucleic acids. When the environmental pH changes, the pH sensor undergoes a conformational transition, which results in a change in the reporter's spectroscopic signal, such as fluorescence or surface-enhanced Raman scattering (SERS).[18,19] Notably, regardless of the existence of a molecularly dense environment, this nanoscale conformational transition undergone by the pH sensor occurs independently and instantly, allowing pH variations to be sensed precisely and accurately by each individual pH sensor. However, unlike naturally occurring conformational transitions, the spectroscopic signal can be easily affected by a crowded surrounding environment and other chemical cues, resulting in decreased pH measurement accuracy. Furthermore, because of the optical resolution limit (200–300 nm), the spectroscopic signal reflects the average performance of a large number of pH sensors rather than the performance of individual sensors. Thus, it is highly desirable to measure the conformational transitions of individual DNA-based pH sensors for pH sensing at the nanoscale.

DNA origami-based nanomechanical devices provide an alternative approach for the readout of individual conformational transitions and biomolecular interactions.[20–24] DNA origami involves self-assembling DNA nanostructures with arbitrary shapes and sizes that can be visualized easily and clearly using atomic force microscopy (AFM) or transmission electron microscopy (TEM). Upon integrating DNA origami with natural biomolecules, dynamic nanomechanical devices can be created that switch between defined molecular conformations in response to specific environmental cues. When these distinct shapes or conformations of dynamic nanodevices are used as shape-resolved labels for distinct visualization, this approach enables the sensing of single and localized dynamic transitions for probing specific chemical cues or studying molecular interactions at the single-molecule level in the fields of biology and chemistry.[25–28] For example, Castro and colleagues developed a DNA origami nanocaliper to investigate chromatin rearrangement in target DNA.[29] These remarkable

[a] *Institute of Molecular Medicine, Shanghai Key Laboratory for Nucleic Acid Chemistry and Nanomedicine, Renji Hospital, School of Medicine, Shanghai Jiao Tong University, Shanghai, 200127, China. E-mail: maoxiuhai@sjtu.edu.cn*
[b] *College of Chemistry and Chemical Engineering, Qufu Normal University, Qufu, 273165, Shandong, China*
[c] *School of Chemistry and Chemical Engineering, Frontiers Science Center for Transformative Molecules and National Center for Translational Medicine, Shanghai Jiao Tong University, Shanghai, 200240, China*
[d] *Division of Physical Biology, CAS Key Laboratory of Interfacial Physics and Technology, Shanghai Institute of Applied Physics, Chinese Academy of Sciences, Shanghai, 201800, China*

† Electronic supplementary information (ESI) available. See DOI: 10.1039/d1cc06701j

‡ These authors contributed equally.

achievements in probing distinct molecular conformational transitions suggest compelling applications in the area of pH sensing at the nanoscale.

Herein, we report the combination of a DNA origami nanomechanical device with TEM imaging for pH sensing at the nanoscale. We constructed a DNA origami nanocaliper with pH-responsive triplex DNA integrated into its two arms. Our incorporation scheme couples the nanocaliper angle to the conformational transition of triplex DNA, such that the hinge angle of the nanocaliper, when imaged using TEM, serves as a shape-resolved label for reporting local pH variations. First, we found that the nanocaliper retains its structural distinctiveness and integrity in a variety of environmental systems, including at high salt concentrations, in the presence of molecular crowding, and under acidic conditions. Following that, we examined the hinge angle of the nanocaliper in relation to the solution pH. The hinge angle was found to be an accurate indicator of pH variations. As a proof of concept, we demonstrated that the device is capable of sensing subtle differences in local pH near carbon nanotubes (CNTs) with nanoscale resolution. These studies demonstrate the feasibility and potential of using this shape-resolved nanocaliper to sense local pH or other biological cues at the nanoscale.

To sense local pH at the nanoscale, we designed a DNA origami nanocaliper that relies on the structural dynamics of triplex DNA (Fig. 1). This nanocaliper is composed of two stiff arms that measure 34 and 44 nm in length from pivot to end (Fig. S1, ESI†). To detect changes in the local pH, the nanocaliper is hybridized with pH-responsive triplex DNA, which is attached to each arm. Under acidic conditions, the triplex DNA hybridizes ssDNA to dsDNA *via* Hoogsteen bonds in its major groove (Fig. S2 and S3, ESI†). The nanocaliper conformational transition results in a significant decrease in its hinge angle. Meanwhile, using TEM imaging, this shape transition of the DNA origami nanocalipers can be easily and clearly visualized. Thus, we can directly observe the distribution of hinge angles based on each individual nanocaliper surrounding the target material using TEM imaging to determine the local pH at the nanoscale.

The DNA origami nanocaliper was first assembled in a typical formation solution containing 12.5 mM Mg^{2+}. Electrophoresis shift analysis confirmed the nanocaliper assembly, as the nanocalipers exhibited only one band with identical mobility at pH values of 5.0 and 7.4, respectively (Fig. S4, ESI†). Additional nanoparticle tracking analysis (NTA) revealed that the formed nanocalipers have a single peak at 70 nm in their size distribution, matching the size of an individual nanocaliper based on our design (Fig. S5, ESI†). Notably, this size distribution result implies that individual nanocalipers disperse freely in both weakly acidic and basic solutions. Taken together, these results demonstrate that the nanocaliper can self-assemble efficiently and remain stable in both weakly acidic and basic environments.

Given that the hinge angle serves as a shape-resolved readout for the conformational transition of triplex DNA, the distinctiveness of the hinge angle and the DNA origami arm bundle directly affects the accuracy of pH sensing.[30,31] Therefore, using TEM imaging, we determined the distinctiveness of the assembled DNA origami nanostructures (without triplex DNA) (Fig. S6, ESI†). Specifically, we observed that the DNA origami nanostructures are distributed randomly without aggregation in TEM images, which is consistent with the NTA analysis results given above. Notably, this dispersed distribution of individual DNA origami nanostructures allows for the accurate measurement of the hinge angle independent of the influence of other nanocalipers. Meanwhile, we found that both arms of the DNA origami nanostructure have a nearly identical width of 10 nm, indicating that they can be easily observed and selected using transmission electron microscopy (TEM) images.

To further assess the distinctiveness of the nanocalipers in different environmental systems, we examined their structural integrity under high-salt conditions (40 mM Mg^{2+} and 0.8 M Na^{+}) and in a highly crowded molecular environment (5% PEG), respectively. We found that they exhibited identical mobility under all conditions, demonstrating that these nanocalipers are stable in these complex microenvironments (Fig. S7, ESI†). Next, we validated their structural distinctiveness and integrity *via* visualizing their morphologies and shapes using TEM imaging. Specifically, we observed that all DNA origami nanostructures exhibited V-shaped arm bundles with an identical width (10.3 nm) and an identical average hinge angle of 78° (Fig. S8–S11, ESI†). These results clearly demonstrate that a complex environment has a negligible effect on the nanocaliper integrity and distinctiveness. As a result, we can identify isolated single nanocalipers and precisely measure their hinge angle using TEM imaging, thereby enabling the DNA origami nanocalipers to be used as distinct shape-resolved labels.

The pH sensing method is based on the change in the hinge angle caused by the dynamic transition of triplex DNA in response to pH variations.[32,33] To determine the nanocaliper response to local pH, we investigated the pH responsiveness of the nanocaliper *via* plotting its fluorescence intensity across a range of pH values. Specifically, the conformational change of the nanocalipers results in a change in the fluorescence signal due to the FRET effect, which is sensitive to the distance between the FRET pair (Cy3 as a donor and Cy5 as an acceptor) at the ends of triplex DNA. As illustrated in Fig. 2b, the fluorescence exhibited a characteristic sigmoidal curve with a

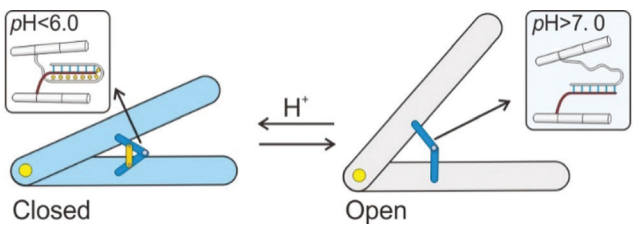

Fig. 1 The design and assembly of the DNA origami nanocaliper with pH-responsive triplex DNA. Triplex DNA works as a responsive actuator module toward local pH, extending from the centers of the two arms of the origami bundle.

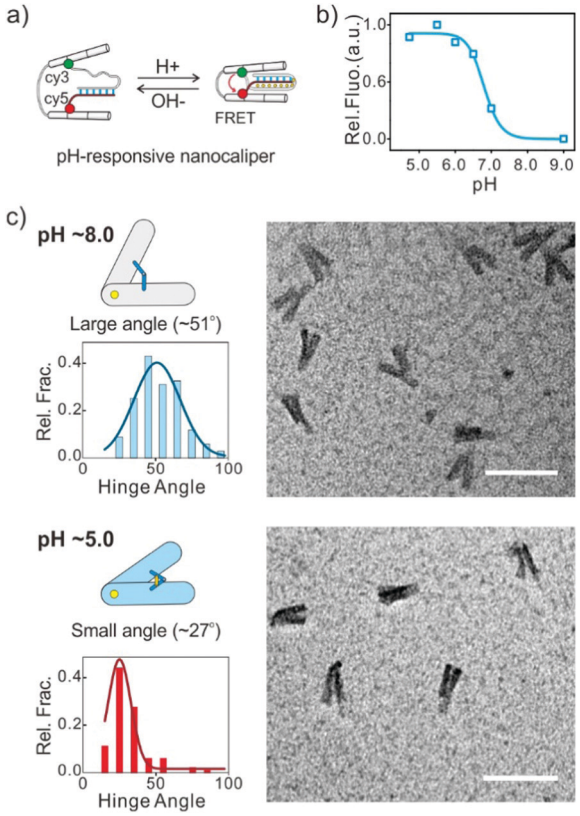

Fig. 2 The pH responsiveness of the DNA origami nanocalipers. (a) A schematic representation of the pH-responsive DNA origami nanocaliper. (b) Cy5 fluorescence intensity analysis of the nanocaliper at different pH values. (c) TEM imaging and conformational analysis of nanocalipers and their hinge angles at pH values of ~5.0 and ~8.0; scale bar: 100 nm. At a pH value of ~8.0, the nanocalipers exhibited a broad angular distribution, ranging from 20° to 120°, with a relatively flat maximum ranging from 35° to 70°. At a pH value of ~5.0, a maximum magnitude occurs at around 21°.

folding/unfolding midpoint (pK_a) of 6.5, which was nearly identical to that of native triplex DNA (Fig. S12, ESI†). Notably, the slope of the fluorescence curve between pH 6.0 and 7.0 is measured to be 2, demonstrating its extreme sensitivity to localized pH variations.

After demonstrating the nanocaliper pH responsiveness, we determined their accuracy in relation to pH sensing at the nanoscale *via* observing their conformational transition at the single-molecule level. We observed and measured the hinge angle of this structure using TEM imaging under both acidic (5.0) and basic (8.0) conditions. As seen in Fig. 2c, statistical histograms of the nanocaliper hinge angle are presented based on an assessment of 100 individual samples at pH 5.0 and 8.0, respectively. We observed that the nanocaliper distribution has a relatively clear maximum at an angle of 51 ± 16° and a full width at half maximum (FWHM) of 37° at pH 8. As the solution enters an acidic state (pH 5.0), the angle distribution exhibits a significant shift and significant narrowing, with an average maximum at approximately 27 ± 8° and a FWHM of 18°. These results were also confirmed *via* AFM imaging (Fig. S13 and S14, ESI†), demonstrating that the formation of triplex DNA under acidic conditions results in a decrease in the nanocaliper hinge angle. This implies that the nanocaliper hinge angle is an accurate chemical indicator of local pH at the single-molecule level.

The pH responsiveness of this nanocaliper, when combined with the nanometer imaging resolution of TEM, enables direct local pH sensing relating to nanomaterials. Given that negatively charged nanomaterials can attract hydrogen ions to their surfaces as a result of the surface potential effect,[4] we focused on the *in situ* probing of subtle differences in the local pH values of nanomaterials using nanocalipers and TEM. For instance, carbon nanotubes (CNTs) are a well-ordered, all-carbon, hollow graphitic nanomaterial with a wide range of electronic properties.[34–36] CNTs have been shown to promote the formation of i-motif DNA.[37,38] Although simulation studies demonstrated that non-specific DNA–SWNT interactions in water are caused by nucleic acid–base stacking on the nanotube surface, it remains unknown whether pH variations in the localized microenvironment have significant effects on the formation due to a lack of *in situ* pH measurements near CNTs.

We used our nanocalipers to determine the local pH of carbon nanotubes as a proof of concept. Specifically, we incubated carbon nanotubes with nanocalipers in Tris buffer (5 mM Tris, 1 mM EDTA, 12.5 mM $MgCl_2$; pH: ~8.0) and imaged this mixture using TEM (Fig. 3a) and AFM. As illustrated in the TEM images, all carbon nanotubes and nanocalipers are distributed randomly and individually on the TEM grid. Notably, we observed that the majority of nanocalipers located near a

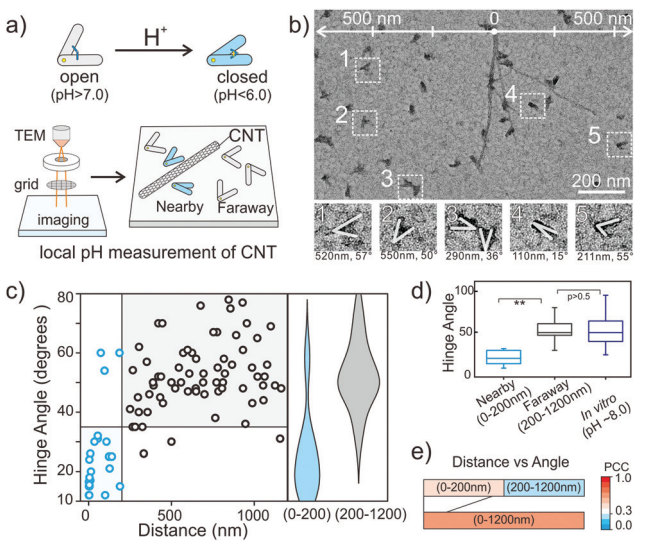

Fig. 3 The *in situ* visualization of pH variations using DNA origami nanocalipers. (a) A schematic diagram of *in situ* pH monitoring. (b) TEM imaging and (c) angle analysis of nanocalipers incubated with CNTs. The nanocalipers within 200 nm of a CNT exhibited an average magnitude of around 23 ± 14°, while the other nanocalipers reveal an average magnitude of around 53 ± 13°. (d) A comparison of the hinge angles of nanocalipers within 200 nm of a CNT and those far away (within 200–1200 nm). *P* values were calculated *via* the one-sample *t*-test. (e) Pearson correlation values between the hinge angle of the nanocaliper and the spatial distance.

CNT had a hinge angle less than 35°, whereas others had a hinge angle greater than 50° (Fig. 3b, c, and Fig. S15, ESI†). Next, we randomly selected nanocalipers (a total of 100 samples) and measured their hinge angles individually from TEM images. The results indicate that the hinge angle is highly dependent on the spatial distance between the nanocaliper and the CNT, and the nanocalipers can be classified into two categories. Specifically, nanocalipers located within 200 nm of a CNT exhibit an average magnitude of around 23 ± 14°, whereas the angular distribution of the other nanocalipers undergoes a significant shift and widening, with an average magnitude of around 53 ± 13°. Moreover, a very similar result was obtained from AFM images (Fig. S16 and S17, ESI†). Notably, Pearson correlation coefficient analysis demonstrates that the hinge angle is strongly related to the spatial distance from a CNT (Fig. 3e). Meanwhile, hinge angle analysis demonstrates that the faraway nanocalipers exhibit an identical angle distribution to nanocalipers in the Tris buffer (Fig. 3d). Thus, the above results demonstrate that the local pH value within 200 nm of a CNT is below 6.0 due to the negative charge of the CNTs.

In this work, we have successfully employed nanocalipers for pH sensing at the nanoscale. The nanocaliper angle generated due to the dynamic transition of triplex DNA serves as an actuated measure of the local pH when the nanocaliper is used as a shape-resolved nanodevice. Owing to its superior addressability and programmability, this molecular nanocaliper can be rationally designed to probe various stimuli *via* incorporating different responding modules, enabling us to better probe complex biological environments with direct visualization at the single-molecule level. Nanomechanical detection systems could find future applications in biosensing and nanomedicine.

This work was supported by the National Key Research and Development Program of China (2018YFA0902600), Natural Science Foundation of Shanghai (21ZR1439600), National Natural Science Foundation of China (22174092, 21904086, 21804091, and 22104086), and the ''Shuguang Program'' supported by the Shanghai Education Development Foundation and Shanghai Municipal Education Commission (Grant 18SG16).

Conflicts of interest

There are no conflicts to declare.

Notes and references

1 J. Zhu, L. S. Hu, P. X. Zhao, L. Y. S. Lee and K. Y. Wong, *Chem. Rev.*, 2020, **120**, 851.
2 P. Kovaricek, M. Cebecauer, J. Neburkova, J. Barton, M. Fridrichova, K. A. Drogowska, P. Cigler, J. M. Lehn and M. Kalbac, *ACS Nano*, 2018, **12**, 7141.
3 W. J. Xuan, Y. H. Xia, T. Li, L. L. Wang, Y. L. Liu and W. H. Tan, *J. Am. Chem. Soc.*, 2020, **142**, 937.
4 Y. Zhang, S. Tsitkov and H. Hess, *Nat. Commun.*, 2016, **7**, 13982.
5 M. Borkowska, M. Siek, D. V. Kolygina, Y. I. Sobolev, S. Lach, S. Kumar, Y. K. Cho, K. Kandere-Grzybowska and B. A. Grzybowski, *Nat. Nanotechnol.*, 2020, **15**, 331.
6 I. Fernando and Y. Zhou, *Chemosphere*, 2019, **216**, 297.
7 R. L. Zhang, F. W. Pratiwi, B. C. Chen, P. Chen, S. H. Wu and C. Y. Mou, *ACS Appl. Mater. Interfaces*, 2020, **12**, 42472.
8 X. Chen, T. Chen, L. Ren, G. Chen, X. Gao, G. Li and X. Zhu, *ACS Nano*, 2019, **13**, 7333.
9 M. T. Ghoneim, A. Nguyen, N. Dereje, J. Huang, G. C. Moore, P. J. Murzynowski and C. Dagdeviren, *Chem. Rev.*, 2019, **119**, 5248.
10 C. Liu, Z. Huang, W. Jiang, X. Liu, J. Li, X. Han, H. Tu, L. Qiu and W. Tan, *Anal. Chem.*, 2020, **92**, 3620.
11 A. Steinegger, O. S. Wolfbeis and S. M. Borisov, *Chem. Rev.*, 2020, **120**, 12357.
12 A. R. Sarkar, C. H. Heo, L. Xu, H. W. Lee, H. Y. Si, J. W. Byun and H. M. Kim, *Chem. Sci.*, 2016, **7**, 766.
13 S. Li, A. W. Zhu, T. Zhu, J. Z. H. Zhang and Y. Tian, *Anal. Chem.*, 2017, **89**, 6656.
14 Z. C. Liu, H. Pei, L. M. Zhang and Y. Tian, *ACS Nano*, 2018, **12**, 12357.
15 T. Patino, A. Porchetta, A. Jannasch, A. Lladó, T. Stumpp, E. Schäffer, F. Ricci and S. Sánchez, *Nano Lett.*, 2019, **19**, 3440.
16 W. Engelen, K. Zhu, N. Subedi, A. Idili, F. Ricci, J. Tel and M. Merkx, *ACS Cent. Sci.*, 2020, **6**, 22.
17 L. Shi, F. Cao, L. Zhang and Y. Tian, *Anal. Chem.*, 2020, **92**, 4535.
18 Y. Hu, A. Cecconello, A. Idili, F. Ricci and I. Willner, *Angew. Chem., Int. Ed.*, 2017, **56**, 15210.
19 C. Zhu, J. Yang, J. Zheng, S. Chen, F. Huang and R. Yang, *Anal. Chem.*, 2019, **91**, 15599.
20 M. W. Hudoba, Y. Luo, A. Zacharias, M. G. Poirier and C. E. Castro, *ACS Nano*, 2017, **11**, 6566.
21 P. W. Rothemund, *Nature*, 2006, **440**, 297.
22 L. Yan, X. Mao and X. Zuo, *Chem. Res. Chin. Univ.*, 2020, **41**, 1415.
23 X. Xin, L. Wang, K. Wang, L. Dai, H. Cao, Z. Li and Y. Tian, *Chem. Commun.*, 2020, **56**, 4918.
24 A. Kuzuya, Y. Sakai, T. Yamazaki, Y. Xu and M. Komiyama, *Nat. Commun.*, 2011, **2**, 449.
25 X. Mao, K. Li, M. Liu, X. Wang, T. Zhao, B. An, M. Cui, Y. Li, J. Pu, J. Li, L. Wang, T. K. Lu, C. Fan and C. Zhong, *Nat. Commun.*, 2019, **10**, 1395.
26 P. Zhang, X. Liu, P. Liu, F. Wang, H. Ariyama, T. Ando, J. Lin, L. Wang, J. Hu, B. Li and C. Fan, *Nat. Commun.*, 2020, **11**, 3114.
27 A. E. Marras, Z. Shi, M. G. Lindell, R. A. Patton, C. Huang, L. Zhou, H. Su, G. Arya and C. E. Castro, *ACS Nano*, 2018, **12**, 9484.
28 H. Xue, F. Ding, J. Zhang, Y. Guo, X. Gao, J. Feng, X. Zhu and C. Zhang, *Chem. Commun.*, 2019, **55**, 4222.
29 J. V. Le, Y. Luo, M. A. Darcy, C. R. Lucas, M. F. Goodwin, M. G. Poirier and C. E. Castro, *ACS Nano*, 2016, **10**, 7073.
30 M. Li, Z. Q. Liu, J. S. Ren and X. G. Qu, *Chem. Sci.*, 2020, **11**, 7479.
31 S. Ghosh, S. Takahashi, T. Ohyama, T. Endoh, H. Tateishi-Karimata and N. Sugimoto, *Proc. Natl. Acad. Sci. U. S. A.*, 2020, **117**, 14194.
32 K. Chen, J. Zhou, Z. Shao, J. Liu, J. Song, R. Wang, J. Li and W. Tan, *J. Am. Chem. Soc.*, 2020, **142**, 12079.
33 E. Del Grosso, G. Ragazzon, L. J. Prins and F. Ricci, *Angew. Chem., Int. Ed.*, 2019, **58**, 5582.
34 H. Sun, J. Ren and X. Qu, *Acc. Chem. Res.*, 2016, **49**, 461.
35 W. Wang, X. Y. Lu, P. Su, Y. W. Li, J. J. Cai, Q. Z. Zhang, M. H. Zhou and O. Arotiba, *Chemosphere*, 2020, **259**, 127423.
36 P. Politzer, P. Lane, J. S. Murray and M. C. Concha, *J. Mol. Model.*, 2005, **11**, 1.
37 Y. Song, L. Feng, J. Ren and X. Qu, *Nucleic Acids Res.*, 2011, **39**, 6835.
38 C. Zhao, K. Qu, C. Xu, J. Ren and X. Qu, *Nucleic Acids Res.*, 2011, **39**, 3939.

